Caliphate Journal of Science & Technology (CaJoST)

ISSN: 2705-313X (**PRINT**); 2705-3121 (**ONLINE**) **Research Article**

Article Info

Received: 9th January 2019

Revised: 15th February 2019

Accepted: 21st February 2019

Department of Physics, Usmanu Danfodiyo University, Sokoto.

***Corresponding author's email:** ismailsaidu258@gmail.com

Cite this: *CaJoST,* 2019, 1, 44-52

Design and Implementation of a Device for the Determination of the Effect of Soiling on Photovoltaic Panel Performance

Ismaila G. Saidu*, Musa Momoh, Hassan N. Yahya and Abubakar U. Moreh

The accumulation of dust on photovoltaic (PV) panel can lead to reduced radiation reaching its surface and possibly leading to hot spot effect. In this paper, a device for studying the effect of soiling on a PV module is described. The device was designed to measure the level of accumulated dust on the surface of the panel (panel soiling), using an infra-red transceiver. The sensor is positioned above the panel, with its infra-red (IR) energy reflected off the panel and captured by a photodiode. The amount of energy detected by the photodiode is directly proportional to the amount of energy reflected off the PV module surface which is also inversely proportional to the amount of dust accumulated. The sensor reading is expressed as a percentage of the reflected energy of the soiled surface to that of a clean surface. A provision is made for the output current, voltage and power of the PV to be measured for every soiling. The measured values (percentage soiling, current, voltage and power) are logged and made accessible *via* Wi-Fi network. When tested the designed measuring devices had accuracies that are more than 90% and the logged data could be accessed on the network.

Keywords: Soiling, Logging, Photovoltaic, Power, Transceiver

1. Introduction

Besides solar panels efficiency and size, there are other factors that affect how much power, solar panels can create. Solar energy output is affected by weather and seasonal variations [1]. There is enough literature to show that the output electrical current of a PV module reduces greatly by soiling, bird droppings, dust, leaves, snow and soot [2], [3]. Dust and soil have adverse effect on the environment through obscuring the irradiance that falls on the module surface [3]. These items tend to alter the solar spectrum that affects the spectrally dependent PV modules [4], [5]. These lead to the reduction in the power output of the module [6]. The rate at which these occur is a function of the climatic condition of a place. While snow may not be a problem in a place like Sokoto, dust at certain periods of the year could have significant effect on PV performance. The amount and nature of dust accumulated on a module is largely determined by factors such as type of local soil, the weather pattern of the place, agricultural activities, level and type of industrialization and transportation [4].

It has been estimated that the losses due to dust and soiling in California could be as high as 25% monthly [5]. Studies have also shown that a single washing in the middle of dry season could reduce the losses due to dust accumulation by as much as 50% [6], [7]. Regular cleaning of modules could therefore improve the energy harvest from modules. Another factor that is of great concern due to dust accumulation is that they tend to produce spots that have varying concentrations of dust particles [4]. The variation in dust spots concentration can cause different transmittance of light into the module which can lead to inhomogeneous shading on the cell [7]. This can trigger the hot spot effect where the operating current of a module exceeds the short circuit current of the affected cell. This effect can cause the cell to become reverse biased leading to dissipation of heat.

The knowledge of how solar spectrum is selectively attenuated by dust can help in the process of better selection of technology under specific dusty environments [7]. In measuring the soiling of a PV module, the method that is generally accepted is to compare the electrical output of the soiled PV with a clean one and express them as ratio of each other [8]. The measurement is usually done simultaneously. In most of the studies on the effect of dust on PV

panels, the procedure used are to measure the weight of the dust and then spread them on the panel [9], [10]. Moreover, most of these experiments are rather done under a controlled environment and may not reflect the actual situation [11]. Most of the studies have been conducted in dusty environments in the Arab countries and not in tropical countries [7] like Nigeria. In this paper, a device is designed to study the effect of soiling on the performance of PV installations by measuring and logging the amount of dust and the corresponding electrical parameters of the PV installation. The study is aimed at acquiring accurate and reliable data relating to soiling of PV systems.

2. Methodology

To achieve the aim, appropriate sensors were used to convert the sensed parameters into a proportional electrical equivalent. The electrical quantity which is either analogue or digital is modified, manipulated and stored as desired using electronic means. The outputs of the analogue sensors were first converted to digital format using analogue to digital (AD) converter before feeding them into a central microcontroller. The basic block diagram of the system is shown in Figure 1.

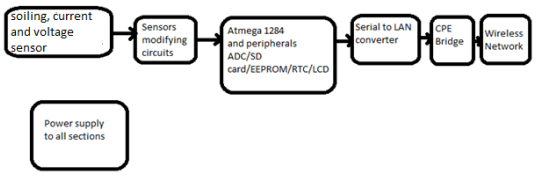

Figure 1. Block Diagram of Soiling Measuring System.

The sensor suit consists of the digital and analogue types. The outputs of both types are fed into the microcontroller after necessary modifications. The microcontroller's peripherals includes a secure digital (SD) card for storing all the logged data, an electrically erasable programmable read only memory (EEPROM) for keeping some key data, real time clock (RTC) chip for keeping real time, analogue to digital converter (ADC) that converts analogue data into digital format, and a liquid crystal display (LCD) unit to display all the vital information.

2.1 Infra-Red (IR) Panel Soiling Measurement Circuit Design

To measure the accumulation of dust on the surface of a panel (panel soiling), an infra-red soiling sensor was used. The sensor is positioned above the panel, with its infra-red energy reflected off the panel to be captured by a photodiode. The amount of energy detected by the photodiode is directly proportional to the amount of energy radiated off the PV module surface. The reflected energy is inversely proportional to the amount of dust accumulated on the module. The sensor reading was evaluated as a percentage of the reflected IR energy of a clean surface. To achieve this, the value of the energy radiated from the panel when the panel is clean is measured and used as the reference radiation (R_r). The Radiation under soiling conditions were measured and recorded as R_c and by using equation 1 the values of the instantaneous percentage soiling (PIR) of the panel were established:

$$PIR = \frac{R_c}{R_r} \times 100 \qquad (1)$$

2.1.1 Circuit Design of IR Transmitter

The transmitter was designed using an IR light emitting diode (LED). The circuit needs to radiate an IR signal of constant magnitude to be reflected by the panel. The circuit is as shown in Figure 2.

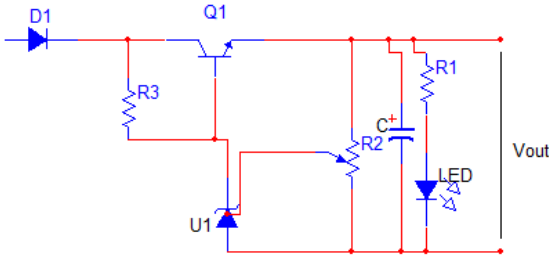

Figure 2. Circuit Diagram of IR Transmitter

Where diode D_1 is a polarity reversal protection diode.

U_1 is aTL431 adjustable Zener regulator.

R_1 biases Q_1 to proper operation range.

R_2 is potentiometer to set the output voltage.

(V_{out}) using the relationship [12]:

$$V_{out} = 2.5\ (1+\frac{R_{2a}}{R_{2b}}) \qquad (2)$$

R_3 is a current limiter resistor to determine the current reaching the IR diode

The diode characteristics curve shows that there is a linear relationship between the radiant intensity and the current through it. A 5 V regulated supply based on the TL431 adjustable shunt voltage references with guaranteed temperature stability over the entire operating

temperature range was used to design a supply voltage for the IR transmiter.

The IR LED current was fixed at 100mA at a forward voltage of 1.1 V. Normally if an LED diode is operated on a continuous mode the current should not exceed 200 mA and 1 A when pulsed [12]. The voltage output from the regulator, V_L was fixed at 5 V so that:

$$R_3 = \frac{\text{VL} - \text{Forward diode voltage}}{IR\ LED\ Current} \quad (3)$$

$R_3 = \frac{5-1.1}{0.1}$ =39 Ω

R_2 is a potentiometer chosen for a track resistance of 5 k.

So that from equation 1, with Vout as 5 V:

$\frac{R_{2a}}{R_{2b}}$ =1

Setting R_2 midway along the track yielded the desired output voltage of 5 V.

The current handling capacity of the regulator was fixed at 1 A that is 10 times the load current of 0.1 A

The emitter current, $I_E = I_C + I_B$ (4)

But, $I_B = I_{R1} - I_Z$ (5)

I_z, taken from a range specified in the datasheet was fixed at 1 mA

The beta gain of the transistor used was measured to be 48, for this reason, a value of 50 was assumed for the evaluation of the base resistor (R_1).

So that $I_B = \frac{I_C}{\beta}$ (6)

I_{R1}=21 mA

R_1 was evaluated using 7 V as the worst case input operational voltage for regulation and

$$R_1 = \frac{V_{in} - (V_{out} + V_{BE})}{I_{R1}} \quad (7)$$

We obtained a value of $R_1 = \frac{7-5.6}{0.021}$ = 66 Ω.

A value of 100 Ω was chosen.

$P_{R1} = I_{R1}^2 \times R_3$ (8)

A resistor of 100 Ω, 0.25 Watts was chosen.

A 100uF aluminium capacitor was placed across the output rail for improved regulation.

2.1.2 Photo Sensor Circuit Receiver

The reflected signal is to be intercepted by a sensor circuit. A photo diode was used to detect the reflected ray from the solar panel. For this purpose, a BPW34 PIN photodiode with high speed and high radiant sensitivity was used as the sensor to receive the reflected signal. Its main features are high photo sensitivity, high radiant sensitivity and fast response times [13], [14].

A Transimpedance amplifier was designed and used to modify the light-dependent current of the photodiode. Transimpedance amplification is the most common type of signal amplification, where an op-amp and feedback resistor are employed to amplify an instantaneous current as it is excellent for measuring within a fixed decade range [15]. In this design, the gain is kept constant as the transmitted signal should not change for accurate measurement. The design employed a single supply amplifier with consideration of factors including stability and input and output voltage range limitations. A transimpedance amplifier with a feedback resistor (R_f) shown in Figure 3 causes the output voltage to change according to equation 9 [16]:

$$V_{out} = -I_{in} R_f \quad (9)$$

Where I_{in} is the photodiode light signal current

R_f = Feedback resistance

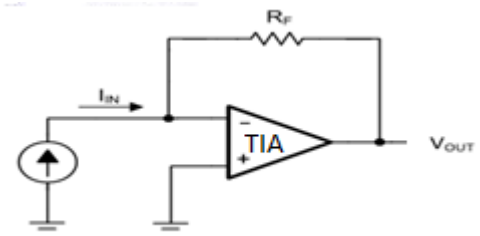

Figure 3. Photodiode with Transimpedance Amplifier

R_f is necessary to ensure that the op-amp operates as a linear amplifier. As shown in the circuit of Figure 2, the photodiode is operated in photoconductive mode so that exposure to light should cause a reverse current through the photodiode. This current causes the op-amp output voltage to increase as well. This is shown in equation (6)

$$V_{out} = I_p R_f \quad (10)$$

The transmitter was placed at 5 cm from the photodiode and the current it generated was carefully measured by connecting the photodiode across a 1 Ω resistor and 5 V supply. The 5 V supply was chosen to match the maximum ADC input voltage. The current measured of approximately 1 mA was used to evaluate the feedback resistor of approximately 5 K. The circuit diagram is shown in Figure 4. The second op-amp circuit is a buffer amplifier with unity gain while the

100 Ω resistor is to prevent shunting of the op-amp.

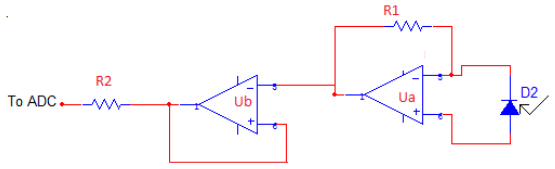

Figure 4. Circuit diagram of the soiling device.

The circuit was constructed and carefully inserted in a plastic pipe as shown in Plate 1.

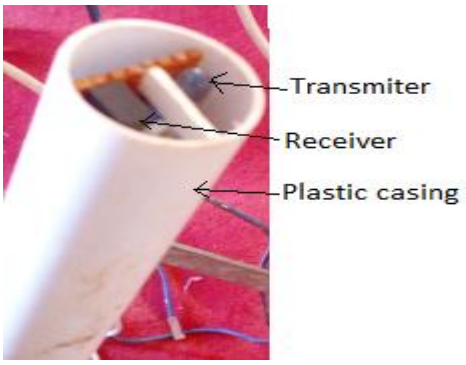

Plate 1. Cased Soiling Device

2.2 Voltage Measurement Circuit

Voltage from the PV array is measured using a simple resistive attenuation network. The voltage to be measured is scaled down using two resistors sized appropriately for the intended application. The consideration was for the circuit to measure voltages up to 100 V. An attenuation, shown in Figure 5, was based on a simple voltage divider rule which was designed so that the maximum voltage input into the ADC on the microcontroller is 5 V.

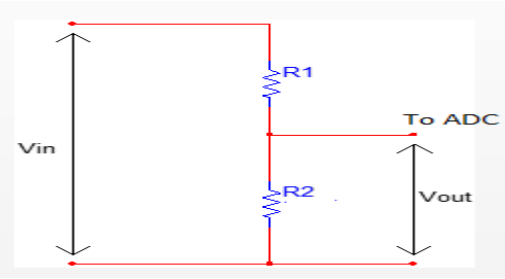

Figure 5. Potential Divider Network for Voltmeter Attenuator

From voltage divider rule:

$$V_{out} = V_{in}\left(\frac{R_1}{R_1+R_2}\right) \qquad (11)$$

With V_{out} given as 5 V and the maximum input voltage at 100 V, assuming R_1 to be 1 MΩ we evaluated the value of R_2 to be 19 MΩ.

2.3 Current Measuring Design Circuit

To assess the performance of the PV installation, there is need for the electrical parameters to be determined. For the current measurement, a Hall Effect current sensor was used. One very popular current sensor is the Allegro ACS758 family of current sensor ICs. The IC is suitable for both AC and DC measurements and finds applications in motor control, load detection and management, power supply and DC-to-DC converter control, inverter control, and overcurrent fault detection [17]. The IC has a copper conducting path that is placed very close to the die.

For the electrical connection, a bypass capacitor with a value of 0.1uF is recommended in its datasheet to be connected between terminal 1 and 2 which is the ground terminal of the IC. A feedback resistor in the range of 1 K is also recommended to be connected to the output terminal which is Pin 3 and the capacitor C_2 is a feedback capacitor. The complete designed circuit is shown in Figure 6.

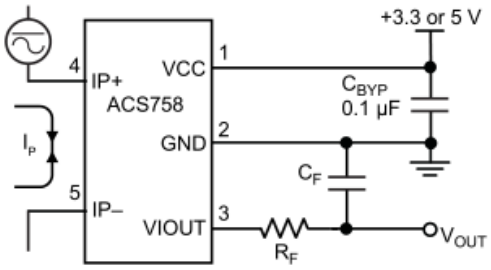

Figure 6. Circuit Diagram of Current Measuring Device.

2.4 Analog-To-Digital Conversion Section

An MCP3208 ADC was used for converting the analog quantities to their digital equivalents. Communication with the device is accomplished using a simple serial interface compatible with the SPI protocol [18]. To increase the resolution of the sampled signals, a selectable oversampling scheme was selected, with oversampling provided for 256x resolution. With oversampling, the resolution of the ADC was effectively improved. The selected oversampling is a trade-off between the slight delay inherent in gathering the required number of samples per analog channel and the speed processing requirement of the system. The ADC was interfaced over PORTA of the ATmega1284 via a four-wire network.

2.5 Ds1307 Serial Real time Clock Chip Section

The requirement to time-stamp measured parameters demanded the need to have a high-accuracy timekeeping management scheme. This was designed around the Ds1307 RTC chip. The DS1307 Serial Real-Time Clock is a low-power, full binary-coded decimal (BCD) clock/calendar plus 56 bytes of NV SRAM. Address and data are transferred serially via a 2-wire, bi-directional bus [19]. Since the RTC device is I²C compatible, it was configured as a slave in the two-wire bus. The RTC circuit connection is shown in Figure 7.

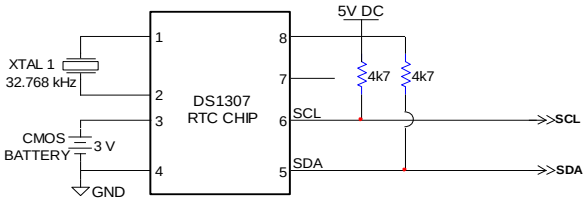

Figure 7. The RTC Circuit diagram

The 32.768 KHz crystal was connected between pins 1 and 2 of the RTC chip as recommended in its data sheet. Two pull up resistors with values of 4K7 were used to pull the serial data line (SDC) and serial clock line (SCL) terminals 6 and 7 to the 5V supply rail. To make provision for a redundant power supply, a 3V Lithium battery is as recommended in the data sheet of the IC [19]. It is recommended that the value of the battery must be between 2.5 and 3.5 volts for proper operation. The nominal write-protect trip point voltage (the maximum number of nodes) is limited by the address space. The two 4.7 K resistors are normal pull up resistors since the 1²C uses two bidirectional open-drain lines. In this design, the microcontroller serves as the only master while the DS1307 and AT2408 are slaves.

2.6 24C02 Serial EEPROM Circuit

The system utilized external non-volatile reprogrammable memory device to store system configuration data. The configurations were saved to and loaded from a serial electrically erasable programmable read only memory (EEPROM). The 24C02 EEPROM has 256 bytes of quick-programming EEPROM cells and its circuit is shown in Figure 8.

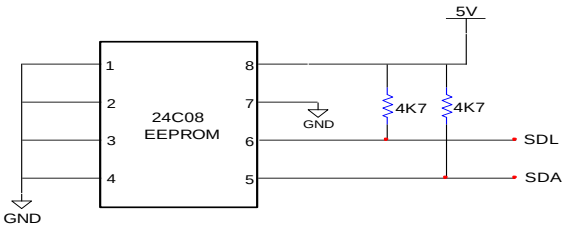

Figure 8. The EEPROM connection circuit.

The EEPROM shared the same 2 wire bus with the RTC circuit to avoid multiple bus system.

As recommended in the data sheet [20], pins 1 to 4 and 7 were grounded. The chip requires a supply of between + 4.5V to 5.5V power supply. A dc power of 5V was therefore used to power the device. Two pull up resistors were also used to tie the communication lines to the supply rail.

2.7 WIZ1000 Serial-To-Ethernet Converter Section

Due to the need to interface the microcontroller with an Ethernet network a physical-layer device was required to translate TTL/RS232 data to IEEE 802.13 packet protocol. The serial-to-Ethernet conversion was effected using a WIZ1000 device server which acts as a gateway between RS232 and Ethernet. It enables remote gauging, managing and control of a device through the network based on Ethernet and TCP/IP by connecting to the existing equipment with RS232 serial interface [21]. The WIZ1000 is essentially a protocol converter that transmits the data sent by a serial equipment as TCP/IP data type and converts back the TCP/P data received through the network into serial data to transmit to the equipment.

2.8 Secure Digital (SD) High-Capacity Storage Section

For long-term historical storage of environmental data, a rugged and high-capacity storage medium was required. Based on the need for easy interfacing with a computer system, a Secure Digital (SD) card was used. The high-capacity card was interfaced *via* PORTB of the ATmega1284 as it features the hardware Serial Peripheral Interface (SPI) communication interface. The SPI bus was configured for 8MHz operation. The SD Card Physical Connections is shown in Figure 9 as recommended by the datasheet of the card.

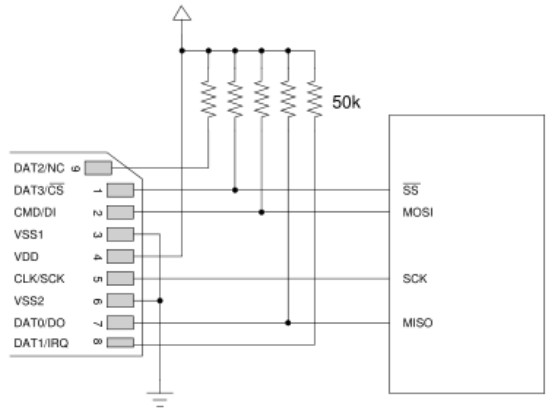

Figure 9. SD card andMicrocontroller interface [22].

2.9 Tplink TL-WR541G 54M Wireless Router

To provide wireless connectivity to client computers, a wireless networking infrastructure was integrated. The wireless inteface comprised the WIZ1000 and a TPLink 54Mbps access point. The WIZ1000 funneled serial-to-ethernet packets over a Local Area Network (LAN) port on the Dlink to be transmitted over the wireless link (Plate 2). The TL-WR541G 54Mbps Wireless Router integrates 4-port Switch, Firewall, NAT-router and Wireless AP [23].

Plate 2. TPLink TL-WR541G Router [23].

2.10 System Operational Firmware

The system requires integration of and between the different system components using software. A microcontroller was used for this purpose. The pin configuration of the IC is as shown in Figure 10

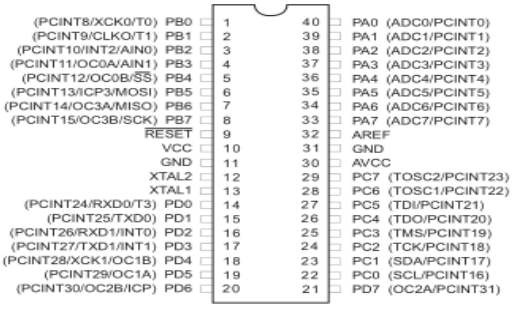

Figure 10. Pin Configuration of ATmega 1284 [24]

The electrical requirement as specified in its data sheet are two separate voltage lines for the analogue and digital signals. The analogue voltage is for the ADC circuit and it is suggested that the value should not be greater than 5V and was sourced from $V_{cc.}$ To minimize or ensure analogue noise cancelling in the circuit as a result of digital signal an external capacitor of 100nF was connected between the analogue supply terminals of the chip as shown in Figure 11. The supply voltage for the digital signal is specified to be between 4.5 and 6.5 volts. A 5V regulated supply was used as the V_{cc} of the circuit.

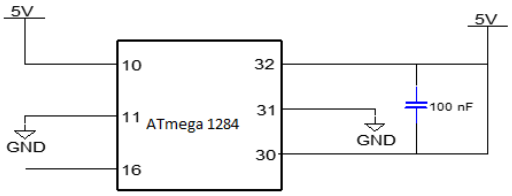

Figure 11. ATmega1284 Supply Circuit

Pin 12 and Pin 13 are the inputs of an external crystal input connected to an inverting amplifier and it is configured as an On-chip oscillator as shown in Figure 12.

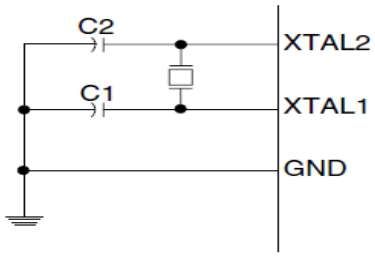

Figure 12. Oscillator circuit of ATmega 1284 microcontroller

The ATmega1284 data book recommends that the values of the capacitors be in such a manner that $C_1 = C_2$ with a value between 12 and 22 pF and a frequency of 32.768 KHZ [24].

The operational firmware was developed and loaded onto a microcontroller [24]. The program, or source code, was written in Microsoft Notepad and then translated by an assembler program to produce the output as an object code for the microcontroller to execute. After the program was compiled, it was recorded in the FLASH EEPROM and the microcontroller runs it itself after a reset or powering on, even without an auxiliary computer. The microcontroller was programmed using ICC AVR C compiler and development studio. The compiler was chosen as it supports

standard C libraries with optimized code footprint and reasonable execution speed on the 8-bit microcontroller.

The microcontroller was programmed to execute the following tasks in an infinite loop:

1. Read sensor data
2. Average sensor data over measurement interval
3. Format averaged sensor data as .CSV string
4. Append to existing file, create one if none found
5. Detect client HTTP request
6. Service HTTP request and return response to client

The firmware for the microcontroller was compartmentalized for ease of easy testing, debugging, and modifications. The C language source code was assembled into Hex File using the ICC AVR Compiler. The Hex File containing the op-codes in Hex-ASCII was then transferred to the microcontroller using a parallel programmer.

2.11 MAX232 TTL-RS232 Logic Level Converter Section

The ATmega1284 microcontroller used in the system is a single-voltage device, the WIZ1000 Serial-to-Ethernet Converter integrated within the system operates using bipolar voltages. The translation between the logic level requirements was effected using a MAX232 level converter. This device converts between microcontroller TTL voltages and WIZ1000 bipolar voltages. This conversion ensured communication between the two data communication entities. As recommended in the datasheet of MAX232 application note [25], the circuit of Figure 13 was adopted.

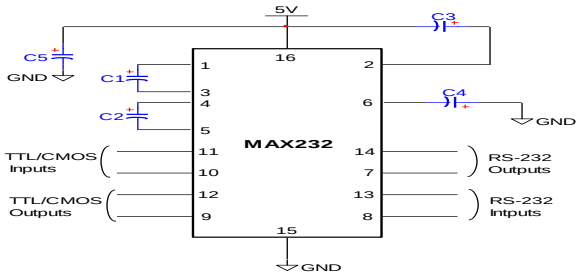

Figure 13. MAX 232 Circuit Connection Diagram

A 5 V stabilized dc supply was used to power the device with the + 5 V at Pin 16 while the ground was connected to Pin 15. Vcc is decoupled to the ground with capacitors C_1 and C_2 to prevent noise. The data sheet of the device recommends that $C_1 = C_2 = C_3 = C_4 = 0.1\mu f$ [25]. In operation, Terminal 9 serves as the receiving terminal while data is transmitted through Pin 10.

After the construction was completed, the device was placed above a clean surface at exactly 50cm from the panel surface. The voltage generated was measured and recorded as the reference voltage V_r. The voltage measured is then recorded as V_m. The microcontroller is programmed to compute the percentage ratio of V_m to V_r. A provision is made for the value of the reference voltage to be altered by the user which makes the device very flexible as it allows one to define his reference clean surface.

2.13 Circuit Construction

After the circuit design, the components were carefully soldered on Vero board with tests at various stages to ascertain the working conditions of the components and circuits. The constructed device is as in Plate 3.

Plate 3. Constructed Circuit of the Monitoring System.

2.12 Performance Test of Soiling Device

The voltmeter and ammeter, fabricated, were used to compare those of standard equivalents by using them to measure the same quantities. To do these, the two voltmeters (reference and fabricated) were used to measure the open circuit voltages of a PV installation at Umaru Ali Shinkafi Polytechnic, Sokoto. Almost immediately after the open circuit voltage was measured, the voltmeters were disconnected and the two ammeters (reference and fabricated) were used to measure the short circuit current of the same PV installation. The results were then tabulated and used to plot graphs to show the accuracy and correlation.

To test for the performance accuracy of the system, the soiling device was placed in the sun and the transceiver hung rigidly at 20 cm from the

surface of a panel. The panel surface was sprinkled with different amount of fine dust. At each dust measure, the amount of soiling ratio and corresponding current and voltage outputs of the panel were logged.

3. Results and Discussion

3.1 Results

The plot in Figure 14 compares the fabricated voltmeter A to a reference type B. The plot is linear with R^2 value of almost 99%. The equation relating the two is $V_A = 0.122 + 1.002\ V_B$.

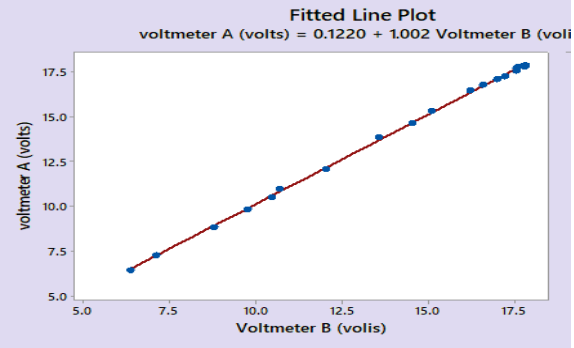

Figure 14. Plot of the Result of the Voltmeter Test

The results obtained from the test to ascertain the accuracy of the ammeter is plotted in Figure 15. The result just like the voltmeter plot shows a linear relationship between the two ammeters with a very high correlation coefficient.

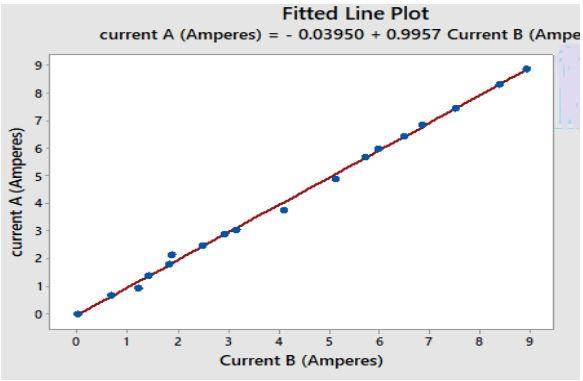

Figure 15. Graph of the Result of the Ammeter Test

The result of the test to determine the ability of the device to measure the soiling on a PV is tabulated in Table 1.

Table 1. Result of the Soiling Test

Soiling ratio	Current (Amperes)	Voltage (Volts)
0.13	1.84	17.43
0.24	3.35	16.64
0.35	4.03	16.40
0.38	4.30	16.29
0.41	4.60	16.18
0.43	5.09	16.60
0.44	5.15	15.89
0.43	5.53	16.30
0.56	5.60	16.33

3.2 Discussion

The voltage measurement test outcome as plotted in Figure 14 indicates a near perfect relationship between the fabricated and reference voltmeters. The R^2 value of 0.99 should be good enough for our purpose. The equation relating the two quantities also show that non-linearity error is also very small. The range of the measurement by the voltmeter is also adequate for the intended use. The current measuring accuracy test indicates a near perfect relationship between the fabricated meter and a standard reference as could be seen from the correlation coefficient of 0.99. The equation relating the two quantities was obtained as current A (Amperes) = - 0.03950 + 0.9957 current B (Amperes). This shows a good linear relationship implying that the fabricated device is accurate and reliable enough. The 0.9957 in the equation shows that there is almost one to one matching of the results of the two quantities measured. The range of measurement extends from zero to 9A for the reference and the fabricated type. The datasheet of the Hall Effect sensor shows that the device could measure from milliamp to hundreds of amperes [17]. The result of the soiling test shows that as the dust level is increased the soiling ratio changes and this affects the amount of current generated by the PV which affects the power output of the PV [7], [8], [11].

4. Conclusion

The study was undertaken to help provide a device that could conveniently be used to estimate the amount of soiling on a PV installation. In addition, a provision is made to also measure the electrical parameters of the installation under the prevailing soiling condition. The result of the

test to evaluate the accuracy of the devices when compared with standard ones showed that there was good correlation between the two sets of meters with values well above 90%. The device was also able to log and the result accessible on a Wi-Fi network.

Conflict of Interests

The authors declare no conflict of interests.

References

[1] M. George, Z. Bastian, N. Matthew and E. George, *Performance of Photovoltaics Under Actual Operating Conditions, Third Generation Photovoltaics*, InTech, http://www.intechopen.com/books/third-generationphotovoltaics, 2012. [Accessed December 12, 2016

[2]. M. Mani and R. Pillai, "Impact of dust on solar photovoltaic (PV) performance: Research
Status, challenges and recommendations," *Renewable and Sustainable Energy Reviews*, vol. 14, pp. 3124-3131, December, 2010.

[3] D. Goossens and E. V. Kerschaever, "Aeolian dust deposition on photovoltaic solar Cells: the effects of wind velocity and airborne dust concentration on cell performance", *Solar Energy,* vol. 66, pp. 277-289, July, 1999.

[4] M. García, L. Marroyo, M. Lorenzo and M. Pérez, "Soiling and other optical losses in solar-tracking PV plants in navarra," *Photovoltaics Res Appl*, vol. 19, pp. 211-217, 2011.

[5] Hammond R., Srinivasan D., Harris A, Whitfield K., and Wohlgemuth, Effects of soiling on PV module and radiometer performance," Photovoltaic Specialists Conference, Conference Record of the Twenty-Sixth IEEE, pp. 1121-1124, 1997

[6] E. Asl-Soleimani, S. Farhangi, M. Zabihi. "The effect of tilt angle, air pollution on performance of photovoltaic systems in Tehran". *Renew Energy*; 24: 459-69, 2001.

[7] Qasem, "Effect of accumulated dust on the performance of photovoltaic modules" A Doctoral Thesis. Submitted in partial fulfilment of the requirements for the award of Doctor of Philosophy of Loughborough University, 2014. https://dspace.lboro.ac.uk/

[8] C. P. Ryan, F. Vignola F, and D. K. McDaniels, "Solar Cell Arrays: Degradation Due to Dirt," in Proceedings of the American Section of the International Solar Energy Society, Denver, CO, pp. 234–237, 1989.

[9] M.R. Maghamia, H. Hizama, C. Gomes, M. A. Radzia, M. I. Rezadadc and S. Hajighorbani, "Power loss due to soiling on solar panel", *Renewable and Sustainable Energy Reviews* A review journal homepage: Published by Elsevier Ltd. 59 pages 1307–1316, 2016.

[10] C. Zorrilla, M. Piliougine, J. Carretero, P. Bernaola, and I. Carpena, "Analysis of dust losses in photovoltaic modules" World renewable energy congress, Sweden Linkoping 8-13 may, 2011.

[11] A. Kimber, L. Mitchell, M. Nogradi, and H. Wenger, "The Effect of Soiling on Large Grid Connected Photovoltaic Systems in California and the Southwest Region of the United States," in Conference Record of the IEEE 4th World Conference on Photovoltaic Energy Conversion, Waikoloa, 2006

[12] Texas Instruments, "Precision Programmable Reference" TL431 datasheet 2018. www.ti.com

[13] Vishay Semiconductors, "Silicon PIN Photodiode" BPW34 datasheet, 2018. www.vishay.com

[14] Hamamatsu Photonics, Application circuit examples of Si photodiode, total emission measurement of LED, S2387, 2002.

[15] A. Ryer, "Light Measurement Handbook" International Light Inc Technical Publications Newburyport. 1998.

[16] D. Medugu, W, Burari, and A. A. Abdulazeez "Construction of a reliable model pyranometer for irradiance measurements" *African Journal of Biotechnology* Vol. 9 (12), pp. 1719-1725, 22 March 2010.

[17] Allegro Micro Systems, "Thermally Enhanced, Fully Integrated, Hall Effect-Based Linear Current Sensor" ACS758xCB datasheet, 2014. www.allegromicro.com

[18] Microchip Technology Incorporated, "4-Channel/8-Channel 12-Bit A/D Converters with SPI Serial Interface". MCP3204 datasheet, 2008.

[19] Maxim Integrated Products, "Serial, I^2C Real-Time Clock", DS130764 datasheet, 2015.

[20] STMicroelectronics, "Serial EEPROM", 24C08 datasheet, 2019

[21] WIZnet "Serial-To-Ethernet Converter module" WIZ1000 manual 2012

[22] PHILIPS semiconductors SD memory card LM324-NXP datasheet, 2009

[23] TPLink Technologies, "wireless router" TL-WR541G datasheet, 2009

[24] Atmel Corporation, "8-bit AVR Microcontroller" ATmega1284P, 2009

[25] Atmel Corporation "8 max Multichannel RS-232 Maxim Integrated Products" Max232 datasheet, 2010. www.atmel.com.

